Fabrication of three-dimensional multi-protein microstructures for cell migration and adhesion enhancement

Yong Da Sie,[1] Yi-Cheng Li,[2] Nan-Shan Chang,[3,4]
Paul J. Campagnola,[5] and Shean-Jen Chen[1,6,7,*]

[1]*Department of Engineering Science, National Cheng Kung University, Tainan 701, Taiwan*
[2]*Department of Photonics, National Cheng Kung University, Tainan 701, Taiwan*
[3]*Institute of Molecular Medicine, National Cheng Kung University, Tainan 701, Taiwan*
[4]*Neuroscience and Physiology, SUNY Upstate Medical University, NY 13210, USA*
[5]*Department of Biomedical Engineering, University of Wisconsin-Madison, WI 53706, USA*
[6]*Advanced Optoelectronic Technology Center, National Cheng Kung University, Tainan 701, Taiwan*
[7]*Center for Micro/Nano Science and Technology, National Cheng Kung University, Tainan 701, Taiwan*
[*]*sheanjen@mail.ncku.edu.tw*

Abstract: In this study, three-dimensional (3D) multi-component microstructures were precisely fabricated via multiphoton excited photochemistry using a femtosecond laser direct-writing system with proposed repetition positioning and vector scanning techniques. Extracellular matrix (ECM) proteins, such as fibronectin (FN), are difficult to stack and form 3D structures larger than several-hundred microns in height due to the nature of their protein structure. Herein, to fabricate complex 3D microstructures with FN, a 3D scaffold was designed and formed from bovine serum albumin (BSA), after which human FN was inserted at specific locations on the BSA scaffold; in this manner, the fabricated ECM microstructure can guide cells in a 3D environment. A human breast cancer cell line, MDA-MB-231, was used to investigate the behavior of cell migration and adhesion on the fabricated human FN and BSA protein structures. Experimental results indicate that many cells are not able to attach or climb on a 3D structure's inclined plane without FN support; hence, the influence of cell growth in a 3D context with FN should being taken into consideration. This 3D multi-protein fabrication technique holds potential for cell studies in designed complex 3D ECM scaffolds.

OCIS codes: (160.1435) Biomaterials; (190.4180) Multiphoton processes; (110.3960) Microlithography; (220.4000) Microstructure fabrication.

References and links

1. S. J. Morrison and J. Kimble, "Asymmetric and symmetric stem-cell divisions in development and cancer," Nature **441**(7097), 1068–1074 (2006).
2. B. M. Gillette, J. A. Jensen, B. Tang, G. J. Yang, A. Bazargan-Lari, M. Zhong, and S. K. Sia, "In situ collagen assembly for integrating microfabricated three-dimensional cell-seeded matrices," Nat. Mater. **7**(8), 636–640 (2008).
3. M. P. Lutolf and J. A. Hubbell, "Synthetic biomaterials as instructive extracellular microenvironments for morphogenesis in tissue engineering," Nat. Biotechnol. **23**(1), 47–55 (2005).
4. G. R. Souza, J. R. Molina, R. M. Raphael, M. G. Ozawa, D. J. Stark, C. S. Levin, L. F. Bronk, J. S. Ananta, J. Mandelin, M. M. Georgescu, J. A. Bankson, J. G. Gelovani, T. C. Killian, W. Arap, and R. Pasqualini, "Three-dimensional tissue culture based on magnetic cell levitation," Nat. Nanotechnol. **5**(4), 291–296 (2010).
5. S. Kobel and M. P. Lutolf, "High-throughput methods to define complex stem cell niches," Biotechniques **48**(4), ix–xxii (2010).
6. F. Klein, B. Richter, T. Striebel, C. M. Franz, G. von Freymann, M. Wegener, and M. Bastmeyer, "Two-component polymer scaffolds for controlled three-dimensional cell culture," Adv. Mater. **23**(11), 1341–1345 (2011).

7. F. Klein, T. Striebel, J. Fischer, Z. Jiang, C. M. Franz, G. von Freymann, M. Wegener, and M. Bastmeyer, "Elastic fully three-dimensional microstructure scaffolds for cell force measurements," Adv. Mater. **22**(8), 868–871 (2010).

8. D. Kim and P. T. C. So, "High-throughput three-dimensional lithographic microfabrication," Opt. Lett. **35**(10), 1602–1604 (2010).

9. Y.-C. Li, L.-C. Cheng, C.-Y. Chang, C.-Y. Lin, N.-S. Chang, P. J. Campagnola, C. Y. Dong, and S.-J. Chen, "High-throughput fabrication of gray-level biomicrostructures via temporal focusing excitation and laser pulse control," J. Biomed. Opt. **18**(7), 075004 (2013).

10. Y.-C. Li, L.-C. Cheng, C.-Y. Chang, C.-H. Lien, P. J. Campagnola, and S.-J. Chen, "Fast multiphoton microfabrication of freeform polymer microstructures by spatiotemporal focusing and patterned excitation," Opt. Express **20**(17), 19030–19038 (2012).

11. S. Kawata and H.-B. Sun, "Two-photon photopolymerization as a tool for making micro-devices," Appl. Surf. Sci. **208–209**, 153–158 (2003).

12. W.-S. Kuo, C.-H. Lien, K.-C. Cho, C.-Y. Chang, C.-Y. Lin, L. L. H. Huang, P. J. Campagnola, C. Y. Dong, and S.-J. Chen, "Multiphoton fabrication of freeform polymer microstructures with gold nanorods," Opt. Express **18**(26), 27550–27559 (2010).

13. P. J. Campagnola, D. M. Delguidice, G. A. Epling, K. D. Hoffacker, A. R. Howell, J. D. Pitts, and S. L. Goodman, "3-dimensional submicron polymerization of acrylamide by multiphoton excitation of xanthene dyes," Macromolecules **33**(5), 1511–1513 (2000).

14. J. D. Pitts, P. J. Campagnola, G. A. Epling, and S. L. Goodman, "Submicron multiphoton free-form fabrication of proteins and polymers: studies of reaction efficiencies and applications in sustained release," Macromolecules **33**(5), 1514–1523 (2000).

15. X. Chen, Y.-D. Su, V. Ajeti, S.-J. Chen, and P. J. Campagnola, "Cell adhesion on micro-structured fibronectin gradients fabricated by multiphoton excited photochemistry," Cell Mol. Bioeng. **5**(3), 307–319 (2012).

16. V. Ajeti, C.-H. Lien, S.-J. Chen, P.-J. Su, J. M. Squirrell, K. H. Molinarolo, G. E. Lyons, K. W. Eliceiri, B. M. Ogle, and P. J. Campagnola, "Image-inspired 3D multiphoton excited fabrication of extracellular matrix structures by modulated raster scanning," Opt. Express **21**(21), 25346–25355 (2013).

17. J. Lu, W. Min, J.-A. Conchello, X. S. Xie, and J. W. Lichtman, "Super-resolution laser scanning microscopy through spatiotemporal modulation," Nano Lett. **9**(11), 3883–3889 (2009).

18. D. S. Correa, M. R. Cardoso, V. Tribuzi, L. Misoguti, and C. R. Mendonca, "Femtosecond laser in polymeric materials: microfabrication of doped structures and micromachining," IEEE J. Sel. Top. Quantum Electron. **18**(1), 176–186 (2012).

19. M. Malinauskas, M. Farsari, A. Piskarskas, and S. Juodkazis, "Ultrafast laser nano-structuring of photopolymers: A decade of advances," Phys. Rep. **533**(1), 1–31 (2013).

20. K. Terzaki, E. Kalloudi, E. Mossou, E. P. Mitchell, V. T. Forsyth, E. Rosseeva, P. Simon, M. Vamvakaki, M. Chatzinikolaidou, A. Mitraki, and M. Farsari, "Mineralized self-assembled peptides on 3D laser-made scaffolds: a new route toward 'scaffold on scaffold' hard tissue engineering," Biofabrication **5**(4), 045002 (2013).

21. A. Ovsianikov, S. Mühleder, J. Torgersen, Z. Li, X.-H. Qin, S. Van Vlierberghe, P. Dubruel, W. Holnthoner, H. Redl, R. Liska, and J. Stampfl, "Laser photofabrication of cell-containing hydrogel constructs," Langmuir **30**(13), 3787–3794 (2014).

22. J. Torgersen, A. Ovsianikov, V. Mironov, N. U. Pucher, X. H. Qin, Z. Li, K. Cicha, T. Machacek, R. Liska, V. Jantsch, and J. Stampfl, "Photo-sensitive hydrogels for three-dimensional laser microfabrication in the presence of whole organisms," J. Biomed. Opt. **17**(10), 105008 (2012).

23. S. Rekštytė, M. Malinauskas, and S. Juodkazis, "Three-dimensional laser micro-sculpturing of silicone: towards bio-compatible scaffolds," Opt. Express **21**(14), 17028–17041 (2013).

24. S. Rekštytė, E. Kaziulionyte, E. Balciunas, D. Kaškelytė, and M. Malinauskas, "Direct laser fabrication of composite material 3D microstructured scaffolds," J. Laser Micro. Nanoen. **9**(1), 25–30 (2014).

25. J.-L. Boulnois, "Photophysical processes in recent medical laser developments: a review," Lasers Med. Sci. **1**(1), 47–66 (1986).

26. I. Gibson, D. W. Rosen, and B. Stucker, *Additive Manufacturing Technologies* (Springer, 2010).

27. A. Kaufman, "Efficient algorithms for 3D scan-conversion of parametric curves, surfaces, and volumes," ACM SIGGRAPH Comput. Graph. **21**(4), 171–179 (1987).

28. J. T. L. Thong, K. W. Lee, and W. K. Wong, "Reduction of charging effects using vector scanning in the scanning electron microscope," Scanning **23**(6), 395–402 (2001).

29. S. Basu and P. J. Campagnola, "Properties of crosslinked protein matrices for tissue engineering applications synthesized by multiphoton excitation," J. Biomed. Mater. Res. A **71**(2), 359–368 (2004).

30. N. I. Smith, K. Fujita, O. Nakamura, and S. Kawata, "Three-dimensional subsurface microprocessing of collagen by ultrashort laser pulses," Appl. Phys. Lett. **78**(7), 999–1001 (2001).

31. D.-X. Wang, D.-M. Guo, C.-Y. Jia, and H.-W. Leng, "Slicing of CAD models in color STL format," Comput. Ind. **57**(1), 3–10 (2006).

32. K.-C. Cho, C.-H. Lien, C.-Y. Lin, C.-Y. Chang, L. L. H. Huang, P. J. Campagnola, C. Y. Dong, and S.-J. Chen, "Enhanced two-photon excited fluorescence in three-dimensionally crosslinked bovine serum albumin microstructures," Opt. Express **19**(12), 11732–11739 (2011).

33. S. H. Mousavi and P. Hersey, "Role of caspases and reactive oxygen species in rose Bengal-induced toxicity in melanoma cells," Iran. J. Basic Med. Sci. **10**(2), 118–123 (2007).

34. S. B. Koevary, "Selective toxicity of rose Bengal to ovarian cancer cells in vitro," Int. J. Physiol. Pathophysiol Pharmacol **4**(2), 99–107 (2012).

1. Introduction

Complex components of extracellular matrix (ECM) proteins play important roles in cell biology, including wound-healing and tumor metastasis. They may also form niche circumstances of tissue engineering scaffolds, since these can influence cell adhesion and migration behavior in three-dimensional (3D) surroundings and promote matrix synthesis. In natural biomaterials, there are usually many different kinds of ECM proteins, such as collagen, elastin, laminin (LN), and fibronectin (FN) for 3D niche micro-environments that release cell signals including all kinds of cytokines, as well as growth factor for cell proliferation, survival, and quiescence [1–4]. Accordingly, it can be said that cell behavior is governed by interactions with the cellular environment. Therefore, 3D ECM microstructures holds great potential in many biological applications, such as high-throughput methods to define complex stem cell niches [5] and fully-elastic 3D microstructure scaffolds for cell force measurements [6]. Fibrous collagen or matrigel matrices are commonly used for the study of 3D cell behavior; however, these matrices have random pore sizes and are structurally and chemically ill-defined, which results in discrepancies between cell behavior in vivo and in artificial two-dimensional (2D) environments. Consequently, devices that approximate the structural complexity present in 3D tissues are highly desirable [7].

There are many different configurations for fabricating complex 3D microstructures, which can be roughly classified into two types: mask projection and point-wise scan. With respect to the former, several mask projection configurations have been demonstrated that can fabricate 3D scaffolds via a digital micromirror device or optical mask [8–10]; however, these techniques have poor axial resolution for 3D fabrication due to the unfilled back-focal aperture. In considering the latter, femtosecond laser direct writing (FLDW) with point-to-point scanning has become a versatile tool in the fabrication of tailored 3D micro/nano-devices in the submicron scale [11,12]. FLDW has been employed to fabricate natural 3D structures of covalently crosslinked proteins in conjunction with a photoactivator [13–16]. This technique adopts a pulsed, temporal focused laser beam with a pulse width of few hundred femtoseconds. The high peak power of the ultra-short pulse and tight focusing by a high numerical aperture (NA) objective lens are critical for inducing sufficient multiphoton absorption to achieve high precision fabrication. The Gaussian profile spatial distribution fits the electrical field strength well with a threshold value. In this regard, multiphoton-polymerization/crosslinking must meet the threshold fabrication energy to initiate the process; as such, actual fabricated sizes could be slightly smaller than that defined by the diffraction limit or the point spread function (PSF) Rayleigh resolution, which has also been demonstrated in two-photon laser scanning microscopy [17–19].

With the FLDW technique, numerous materials have been used to fabricate 2D and 3D microstructures for studying biocompatible scaffolds, including many kinds of photosensitive biocompatible hydrogels via 3D fabrication [20–22]. An alternative method is to use biocompatible photosensitive polymers, which is similar to plastic material PDMS (polydimethyl-siloxane) or SU-8 photoresist for fabricating complex 2D and 3D microstructures. The microstructures are then dipped or soaked in peptides or proteins for assembly and absorption, allowing biomaterial scaffolds to be formed [6,23,24]. Although these methods can fabricate good 2D and 3D biocompatible micro-scaffolds, they indirectly use natural proteins, peptide materials, or biocompatible hydrogels. Therefore, how to fabricate complex 3D microstructures with real natural protein as an ECM scaffold is the primary concern of this study.

Practically speaking, the two-photon crosslinking (TPC) process with rose Bengal (RB) as a photoactivator can produce unpaired electrons for protein crosslinking synthesis to fabricate complex biomaterial structures. In doing so, when the fabrication condition is under the same

fabrication energy density and over the energy threshold, the protein monomer fabrication or crosslinking speed is related to the protein concentration and the photoactivator [25]. And so to accelerate large structure fabrication, the scan rate and protein concentration should be increased. However, the opposite is true for RB, since the higher concentration of photoactivator will result in a decrease of the reactive monomer's concentration and also cause the self-quench effect of RB [26]. Moreover, 3D fabrication is expensive when using high concentrations of FN, which themselves are problematic for 3D structure-stacking to heights of several-hundred microns due to the nature of their protein structure. In response, the multi-protein fabrication strategy proposed herein employs condensed bovine serum albumin (BSA) as the 3D scaffold, and then deposits FN at specific locations. However, due to the complexity involved, many factors impact fabrication quality and yield rate including processing parameters, such as power density, material concentration, and optical set up, as well as repetition positioning and laser path optimization; consequently, the algorithm governing laser path programming was taken into careful consideration [27,28]. With the support of 3D multiphoton excited imaging (for precise targeting) coupled with the vector scan technique, multi-material 3D ECM structures can be successfully manufactured. According to the time-lapse results of interactions between human breast cancer cells (MDA-MB-231) and 3D microstructures, the FN protein-embedded structure appeared to assist cell migration and adhesion in 3D environments; nevertheless, fabricating complex 3D scaffolds with pure ECM protein is difficult. Therefore, the proposed 3D multi-protein fabrication technique with its unique capability of precisely processing and manufacturing of large-scale, multi-component, and elegant freeform ECM protein structures could offer great potential in the field of 3D tissue engineering and in vitro biomedical research for simulating in vivo environments.

2. Materials and methods

2.1. Sample preparation

The fabrication solution consisted of BSA (Sigma-Aldrich, USA) and RB photoactivator (Avocado Research Chemicals Ltd, UK) with concentrations of 300 mg/ml and 4mM, respectively; while, the protein FN concentration was 1 mg/ml. The fabrication solution was confined to a small circular silicone rubber chamber sandwiched between a microscope slide and the 0.17 mm cover slip, upon which the microstructures were fabricated. To provide a flat, native, and stable base for protein structure fabrication, the slips were modified as follows. First, they were sonicated in a 1:1000 dilution of detergent (Aldrich Micro 90C) in deionized (DI) water for 15 min, and then washed for 15 min 3 times in DI water. The surface was sequentially dried with nitrogen or argon, oven-dried for 30min at 120 °C, and subjected to plasma cleaner at 0.3 Torr. for 3 min to remove oxide on the surface. The slips were then soaked overnight in a solution of 0.5% (v/v) ODTS (n-Octadecyltrichlorosilane, Gelest, USA) within toluene in an inert, moisture-free environment to form a self-assembled organosilane monolayer. After soaking, the slips were washed 3 times with anhydrous toluene to remove any residual ODTS, dried with nitrogen, and heated for 30 min at 120 °C to complete the formation of the Si-O bond. In some experiments, the silanized slips were immersed in a 10 mg/ml BSA solution for 45 min to form a monolayer base. It should be noted that the BSA monolayer can be used as a nonspecific surface for comparison with the adhesion dynamics of the cells on or off the crosslinked ECM protein structures. After fabrication, the slips were sequentially washed with DI water, treated with UV light for a few days to photobleach the photoactivator dye and sterilized for cell culture. The MDA-MB-231 human breast cancer cell line was grown adherently and maintained in DMEM (Dulbecco's modified Eagle's medium, 90%) containing 10% fetal bovine serum (FBS) at 37°C, 5% CO_2/95% air cultured with DMEM and FBS with penicillin, and sub-cultured with trypsin/EDTA (Gibco-BRL, Gel, USA).

2.2. Femtosecond laser direct writing system

The FLDW system has been described in detail previously [12]. The laser source was a commercial active mode-lock Ti:Sapphire oscillator (Tsunami, Spectra-Physics, USA) with a 100 fs pulse width and 700 nm~1000 nm wavelength at an 80 MHz repetition rate. To overcome the group velocity dispersion of the FLDW system, an SF-10 prism pair (PC-TS-KT, Newport, USA) was used for optimizing the pulse width. Galvanometer scanners (6215H, Cambridge, USA) optically scanned in the *x* and *y* directions, while an acousto-optic modulator (AOM), acting as an optical shutter, rapidly switched the laser beam and pulse number selection on/off. Other key components of this system include an inverted optical microscope (Axiovert 200, Carl Zeiss, Germany), a *z*-axis piezoelectric nano-positioning stage (Nano-F100, Mad City Labs, USA), an oil-immersion objective (40X/NA = 1.3, Carl Zeiss, Germany), dichroic mirrors, photomultiplier tubes (PMT) (H5783P, Hamamatsu, Japan), and a data acquisition (DAQ) card with field-programmable gate array (FPGA) module (PCI-7831R, National Instruments, USA) with a 200 MHz clock.

The single photon counting (SPC) voltage signal was transferred from the PMTs to the FPGA digital I/O through a lab-made discriminator. Selected experimental parameters such as laser power, scanning rate, and sample positioning can be adjusted via the use of a customized LabVIEW program and several electronics interfaces. In this manner, imaging with nonlinear optical signals such as two-photon excited fluorescence (TPEF)/second harmonic generation, as well as 3D microfabrication can be achieved. According to our previous study [12], the maximum two-photon absorption wavelength of RB is around 715 nm; therefore, this wavelength was adopted for the TPC process. To ensure an increased fabrication energy and accelerated throughput with the same laser power, objective numerical aperture, excitation wavelength, and pulse width, while enabling different scan rates for BSA and FN, the fabrication power densities were adjusted to be around 3.4×10^{16} (W/cm^2) and 1.0×10^{17} (W/cm^2) for BSA and FN, respectively [29,30].

2.3. Design-transformation, vector scanning, and repetition positioning

To transform 3D structures into 2D processing patterns via the FLDW system, a 3D model was initially designed with commercial CAD designing tools such as AutoCAD, Pro/E, and Solidworks, and then converted into a stereo-lithography (STL) format output file. The 3D STL file was then read by our LabVIEW code, and converted into sequential 2D bitmap (BMP) format files by a dynamic library link (DLL) slicing program developed via Visual Studio C++ [31]. According to the mesh vertex in the STL ASCIii encoded type, the slicing program determines all intersection vertexes that a slicing plane crosses with the meshes at the current slicing location. Once all slicing intersection vertexes have been determined, the 2D slicing sections can be acquired via connecting and hole-fill processes, the 2D BMP files of which are then downloaded to the FPGA module as laser processing commands. In this manner, the desired 3D structures can be created through conventional raster scan by controlling the AOM switch.

The direction indication of the relative position, obtained via vector scan and laser path programming, can effectively save memory in the DAQ card for path optimization for comparison with conventional raster scan. The 3D tracing algorithm is more complex; and so in brief, the method used here is to slice the 3D STL file into 2D section arrays as mentioned above, and then use our DLL code for 2D vector scanning and laser path programming. Subsequently, the vector scan and laser path file are downloaded to the FPGA module as laser processing commands. Random 3D structures can be created via vector scan by directly controlling rotation of the galvanometer scanners. Compared with conventional raster scanning for arbitrary 3D fabrication or machining, the primary benefit of vector scanning is that non-processed regions are ignored, which reduces processing time. Furthermore, the quality and yield rate can also be improved due to continuous a laser scanning path.

Moreover, with the aid of 3D TPEF imaging, repetitive positioning can be achieved; hence, the system can precisely duplicate laser fabrication for multi-component microstructures [16].

2.4. Cell migration and cell-matrix interaction analysis

To establish an evaluated standard for estimating cell migration at different structures, the optical flow method from Simulink was used to calculate the mass center position of each individual cell. Manual tracking from ImageJ was used to link each individual cell's position according to the image frames; then, Chemotaxis calculated the mean cell velocity and plot the cell migration path. A phase contrast inverted microscope (IRE-2, Leica, UK) with an objective lens (N Plan 10X ph1, Leica, UK) and a differential interference contrast (DIC) inverted microscope (IX83, Olympus, Japan) with the Xcellence image program were used for time-lapse observation. The cells, cultured as aforementioned, were imaged under environmentally controlled conditions with 5% CO_2 and at 37 °C. In all cases, a p-value less than 0.05 (**$p < 0.05$) was deemed statistically significant, less than 0.1 (*$p < 0.1$) was considered slightly statistically significant, and greater than 0.1 ($p > 0.1$) non-significant.

3. Experimental results and discussions

3.1. Cell migration and adhesion on 2D multi-component biopolymer island-bridge structure

Initially, cell behavior on a 2D micro-pattern was investigated to supplement the study of the 3D multi-protein scaffold. To this end, large-scale island-bridge patterns were designed as a proof-of-principle experiment of cell preference between BSA and FN, as shown in the left-top of Fig. 1(a). The total fabrication size was 400×400 μm^2, with an island diameter of 100 μm, and a bridge width of 30 μm. The 2D island-bridge FN structure, with an FN solution concentration of 1 mg/ml, was fabricated on the substrate with the BSA monolayer coating, as described in Sec. 2.1. To observe specific cell interactions with the FN structure and BSA substrate individually, a cell seeding density of 1×10^4 cells/ml was cultured on the structure and substrate, and then incubated for 24 hours. From the phase contrast time-lapse image shown in Fig. 1(a), it can be seen that after 24-hour seeding with 10% FBS in DMEM, and then 24-hour observation with 2% FBS in DMEM, the MDA-MD-231 human breast cancer cells prefer attaching to the FN structure as opposed to the BSA monolayer substrate. Further, the quantitative analysis in Fig. 1(b) indicates that the mean migration velocity of the cells on the FN scaffold is faster than those on the BSA monolayer. Hence, this also implies that ECM proteins such as FN, LN, elastin, and collagen are better candidates for 3D scaffolds in practical consideration. Therefore, both cell adhesion and migration results suggest that ECM proteins are much more important than other materials for bio-scaffold manufacturing. Consequently, FN seems to be a desirable component for the fabrication of bio-mimetic microstructures, with the following experiments further studying cell behavior in the 3D microenvironment.
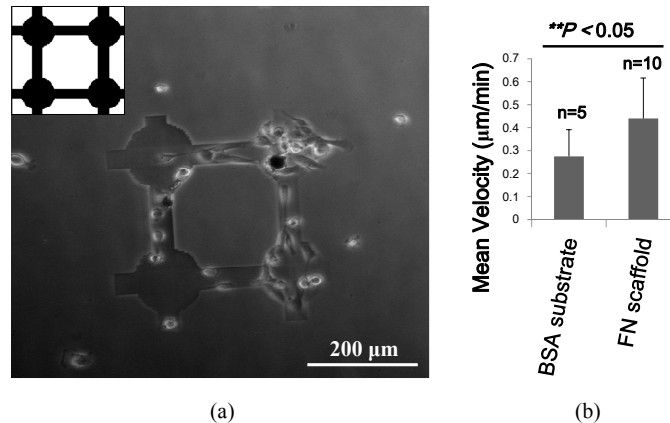
Fig. 1. (a) Phase contrast image of MDA-MB-231 human breast cancer cells migrated on 2D BSA substrate and FN structure 24 hours after cell seeding (Media 1). (b) Quantitative analysis from Media 1 indicates that the cell migration ability on the island-bridge FN structure is better than that on the BSA surrounding substrate. (mean ± standard deviation; Student's *t*-test).

3.2. 3D complex multi-protein microstructures

Herein, a two-step fabrication process using BSA and FN as the artificial 3D bio-structure materials was conducted via vector scanning and repetition positioning in tandem with 3D TPEF imaging. Based on the discussion in Sec. 1 [26], the contained fabrication solution has a higher concentration of BSA than RB. The laser power density on the sample was chosen to be around 3.4×10^{16} (W/cm^2) for BSA and 1.0×10^{17} (W/cm^2) for FN to ensure peak pulse power density over the fabrication threshold value, as illustrated in Sec. 2.2. The pulse width of this ultrafast laser is about 100 fs, which could cause to thermal concerns [25]; therefore, to limit thermal accumulation, the energy density or pixel exposure time can be controlled by either adjusting the scan rate or using the AOM to select the pulse number. In this manner, multi-component fabrication with both BSA and FN can be successfully achieved. Figure 2(a) shows the TPEF images of 4 BSA micro-arches with (left) and without (right) BSA cubes on top. Each fabrication *z*-step was 0.4 μm with a total height of 20 μm. The processing area of 60×60 μm^2 corresponds to 200×200 scanning pixels, i.e. the pixel size was designed to be 0.3 μm relative to the PSF of the focal laser spot. The BSA concentration used here was 150 mg/ml with 4 mM of RB, which is much more condensed than the concentration of FN used. After this initial fabrication step, DI water was used to clear the remaining fabrication solution; then, a TPEF image of the BSA microstructures was obtained via the nonlinear optical microscopy function of the FLDW system and used for repositioning in preparation for the next fabrication step. In the second step, FN with a concentration of 1 mg/ml and 2 mM of RB was utilized to create cubes positioned on the top of the two right-side pre-fabricated BSA micro-arches, as shown in Fig. 2(b). The processing area for the cubes of about 20×20 μm^2 corresponds to roughly 0.3×0.3 μm^2 for each scanning pixel. The TPEF image of Fig. 2(b) demonstrates that the FN cubes were well-formed on the top of the right-side BSA micro-arches structures via the TPC process. As such, the proposed technology is demonstrated capable of fabricating multi-component microstructures with submicron accuracy.

The 3D multi-component fabrication process described above is based on various approaches, including AOM for pulse selection, TPEF imaging for relocation, and vector scanning for path optimization. The complex fabrication material components constitute a superior approach to designing and constructing 3D ECM scaffolds for biomedical research. In addition, we covalently assembled and crosslinked 3D microstructures via two-photon excited photochemistry in our previous study [15,31]. This means that the crosslinked protein

concentration can be modulated by controlling the photon number dosage; therefore, the pulse selector for controlling the protein gradient can increase the complexity and versatility of the practical 3D bio-scaffold, which can also be achieved via this FLDW system.
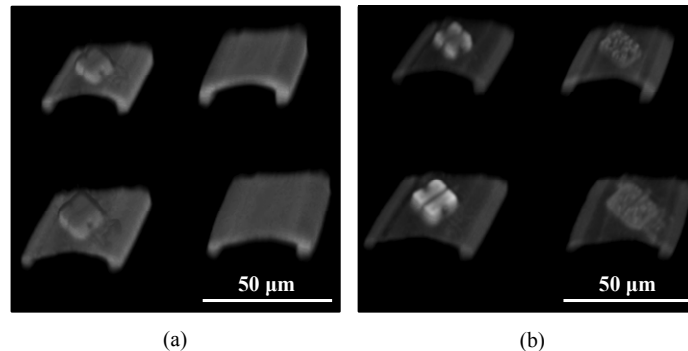

Fig. 2. TPEF images of BSA micro-arches with BSA and FN cubes on top. (a) The initial fabrication step with (left) and without (right) BSA cubes on top (Media 2). (b) After rinsing the remaining solution and injecting FN solution, the second fabrication step adds an FN cube on the top of both right-side BSA structures (Media 3).

3.3.3D BSA/FN microstructures

Based on the above experiments, multi-protein fabrication of 3D scaffolds can be achieved via the FLDW system; subsequently, the fabricated structure can be inspected via the TPEF image of the RB dye remaining in the structure after rinsing in DI water. However, highly condensed RB dye, in addition to producing reactive oxygen species, is an impediment to observations via optical time-lapse microscopy [33,34]. To overcome this issue, before culturing the cells on the fabricated structure, UV light was used to photobleach any condensed RB dye still remaining in the structure. In addition, further washing with DI water can also help diffuse the RB out the structure.

Figure 3(a) illustrates the TPEF image of a fabricated large-scale BSA structure, which was used to study cell migration in a 3D environment without ECM protein support, as discussed in Sec. 3.4. Schematics of the designed structures are shown at the top right of Figs. 3(a) and 3(b). The thickness of each fabricated layer is 0.4 μm, with 200 fabrication layers, yielding a height of 80 μm). The pixel size is 0.3 μm and the processing area covers around 300×300 μm^2. The BSA concentration used here was 300 mg/ml with 4 mM of RB. The structure was designed with a hole in the top's center. The concept of this design was to investigate if the cells inside the cavity interact with the surrounding structure, climb out of the cavity, and migrate on the inclined plane of the cone spontaneously; further, comparisons can then be made with the cell migration outside the structure. Figure 3(b) shows the TPEF image of a second large-scale BSA and human FN hybrid structure. This second BSA/FN multi-component structure was also used to study cell migration in a 3D environment with ECM protein support, as presented in the following section. The top right of Fig. 3(b) shows the hybrid structure's schematic, with gray representing BSA and white indicating FN. The fabrication parameters for the BSA portion were the same as in Fig. 3(a), while the concentration of the FN solution was 1 mg/ml with 4 mM of RB. Figure 3(b) shows the FN successfully coated on the BSA scaffold, forming a 3D FN structure (similar to the 3D island-bridge structure) with the support of the BSA cone backbone. According to our previous study [15], heights of fabricated BSA microstructures can exceed 100 μm; however, this is not workable for LN or FN due to random pore sizes and being structurally and chemically ill-defined. Nevertheless, with this multi-component fabrication technology, complex 3D ECM microstructures can be easily produced via the TPC process.
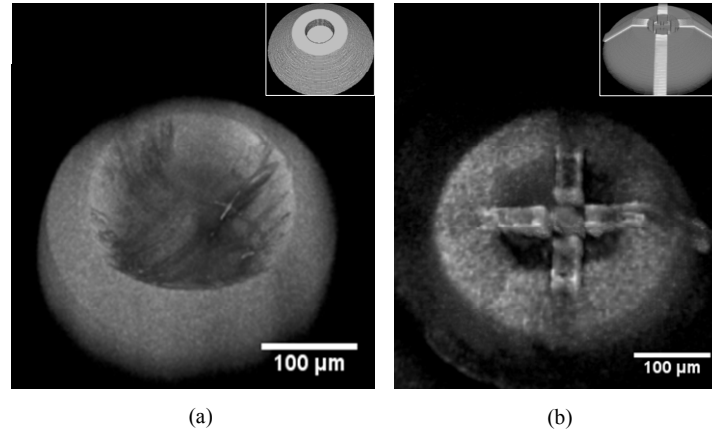
Fig. 3. 3D TPEF images of the fabricated structure bases with diameters of 300 μm and a cavity in the center. (a) Structure fabricated with BSA only. Inset: 3D schematic diagram of the designed structure. (b) Hybrid structure with BSA and FN. FN is formed as a 3D island-bridge structure and placed at a specific location to assist cells to migrate into the central cavity. Inset: 3D schematic diagram of the designed structure with gray representing BSA and white indicating FN.

3.4. Cell migration and cell-matrix interaction analysis

Figures 4(a) and 4(b) show the DIC time-lapse image of cell migrations on the BSA structure and the tracking analysis from the DIC time-lapse video (Media 4), respectively. The BSA structure was identically designed as in Fig. 3(a), and the MDA-MB-231 cells were seeded on the structure for cell migration and climbing in a 3D-enviroment study. The results from Fig. 4(a) and Media 4 show that the cells can remain alive inside the cavity of the BSA structure; however, without ECM protein in the 3D environment, the cells encounter difficulty in attaching and migrating on the inclined plane (Region II) of the BSA structure. The cell-scaffold interaction behavior between the MDA-MB-231 cells and the 3D scaffold were quantitatively analyzed by time-lapse migration measurement over 24 hours after overnight seeding, as shown in Fig. 4(b). Based on the cell migration tracking analysis and cell chemotaxis test, cell migration ability was worse inside the cavity (Region III) than the area surrounding the structure (Region I). The cells inside the cavity could not climb out since BSA has no ECM function bonding domain; hence, the cells were trapped. Be that as it may, the cells can live and growth on the BSA material stereoscopically.

In comparison, Fig. 5(a) presents a phase contrast image and shows that many MDA-MB-231 cells can attach and even climb on the FN-coated inclined plane of the BSA/FN structure shown in Fig. 3(b). As can be seen in the contrast image of Fig. 5(a), the FN is much darker than the BSA. According to the phase contrast time-lapse video results (Media 5), the cells can attach on the 3D FN island-bridge structure and also migrate on the 3D FN scaffold. Moreover, these findings demonstrate that the cells can interact with and adhere to the FN three-dimensionally; however, the cells seldom attached to the BSA, which accords with the results of Figs. 4(a) and 4(b). Further, the cell migration tracking analysis in Fig. 5(b) indicates that the FN structure not only helped cell migration in the 3D environment, but also limited and guided cell migration locationally. Consequently, cell migration ability in the 3D FN structure (Region II) is superior to that in the surrounding area (Region I), as seen in Fig. 5(b) and the part inside the BSA cavity (Region III) of Fig. 4(b).
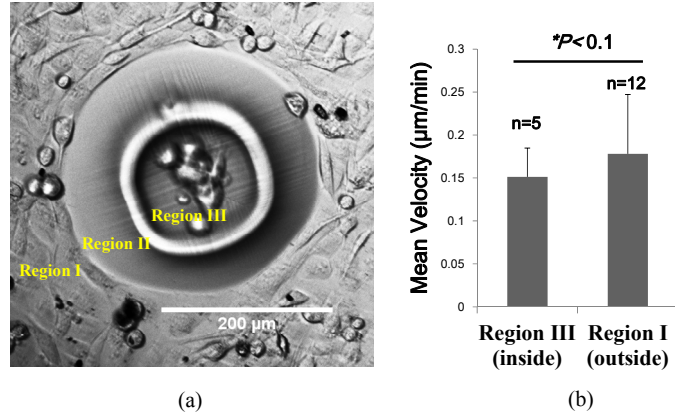
Fig. 4. Human breast cancer MDA-MB-231 cells migrating on the 3D BSA structure after overnight cell seeding. (a) DIC time-lapse image (Media 4); and, (b) cell migration mean velocities for inside the cavity (Region III) and the surrounding area outside the BSA structure (Region I). Cell migration velocity was analyzed using the Student's *t*-test for *p*-value. The bar diagram shows that the mean velocities for the cells inside and outside the structure are 0.151 ± 0.034 (μm/min) and 0.178 ± 0.069 (μm/min), respectively. (mean ± standard deviation; Student's *t*-test)
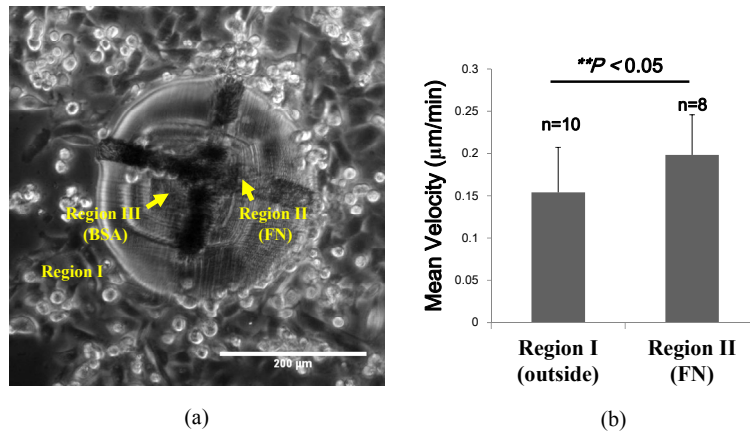

Fig. 5. Human breast cancer MDA-MB-231 cells migrating on the 3D BSA/FN structure after overnight cell seeding. (a) Phase contrast time-lapse image (Media 5); and, (b) cell migration mean velocities for the surrounding area outside the BSA structure (Region I) and the FN island-bridge structure (Region II). Cell migration velocity was analyzed using the Student's *t*-test for *p*-value. The bar diagram shows that the mean velocities for the cells outside the structure and on the FN structure are 0.154 ± 0.053 (μm/min) and 0.198 ± 0.048 (μm/min), respectively. (mean ± standard deviation; Student's *t*-test)

4. Conclusion

This study proposed a FLDW system that integrates repetition positioning and vector scanning techniques to precisely fabricate 3D multi-component microstructures. The optimized laser pathway with vector scanning can increase both the efficiency of the 3D multiphoton fabrication and quality of the complex 3D structure. To fabricate complex 3D microstructures with FN-ECM protein, BSA is first formed into a designed complex 3D scaffold; then, FN is fabricated at specific locations on the BSA scaffold. In this manner, the fabricated ECM microstructure can restrict and guide cells in a 3D environment. The tracking analysis of the MDA-MB-231 cells migration on the protein structures indicates that cells rarely attach or climb on the tilt plane without the support of FN, despite the influence of cell growth in a 3D circumstance with FN being taken into consideration. Accordingly, this

versatile technique holds great potential for fabricating complex 3D ECM scaffolds to study 3D substrate interaction of cell migration and growth.

Acknowledgments